

RESEARCH ARTICLE

Mitochondrial cAMP exerts positive feedback on mitochondrial Ca²⁺ uptake via the recruitment of Epac1

Gergő Szanda^{1,2,*}, Éva Wisniewski¹, Anikó Rajki² and András Spät^{1,2,*}

ABSTRACT

We have previously demonstrated in H295R adrenocortical cells that the Ca²⁺-dependent production of mitochondrial cAMP (mt-cAMP) by the matrix soluble adenylyl cyclase (sAC; encoded by *ADCY10*) is associated with enhanced aldosterone production. Here, we examined whether mitochondrial sAC and mt-cAMP fine tune mitochondrial Ca²⁺ metabolism to support steroidogenesis. Reduction of mt-cAMP formation resulted in decelerated mitochondrial Ca²⁺ accumulation in intact cells during K⁺-induced Ca²⁺ signalling and also in permeabilized cells exposed to elevated perimitochondrial [Ca²⁺]. By contrast, treatment with the membrane-permeable cAMP analogue 8-Br-cAMP, inhibition of phosphodiesterase 2 and overexpression of sAC in the mitochondrial matrix all intensified Ca²⁺ uptake into the organelle. Identical mt-cAMP dependence of mitochondrial Ca²⁺ uptake was also observed in HeLa cells. Importantly, the enhancing effect of mt-cAMP on Ca²⁺ uptake was independent from both the mitochondrial membrane potential and Ca²⁺ efflux, but was reduced by Epac1 (also known as RAPGEF3) blockade both in intact and in permeabilized cells. Finally, overexpression of sAC in the mitochondrial matrix potentiated aldosterone production implying that the observed positive feedback mechanism of mt-cAMP on mitochondrial Ca²⁺ accumulation may have a role in the rapid initiation of steroidogenesis.

This article has an associated First Person interview with the first author of the paper.

KEY WORDS: Mitochondria, cAMP, Ca²⁺ signal, Soluble adenylyl cyclase, Epac, Aldosterone

INTRODUCTION

Aldosterone, which is secreted by adrenal glomerulosa cells, is the principal regulator of salt–water balance. As such, it plays a significant role in the control of blood pressure, and participates in the pathogenesis of cardiovascular, inflammatory and renal diseases (Briet and Schiffrin, 2010; De Mello, 2017; Prabhu and Frangogiannis, 2016; Rossier et al., 2017; Zhang and Lerman, 2017). The most important physiological stimuli of aldosterone secretion are angiotensin II (AngII) and extracellular K⁺, their actions are mediated chiefly by the cytosolic Ca²⁺ signal (Hattangady et al., 2012; Spät and Hunyady, 2004). Cytosolic Ca²⁺, beside inducing and activating

StAR, the steroidogenic acute regulatory protein that transports cholesterol to the inner mitochondrial membrane (IMM) (Cherradi et al., 1997), evokes mitochondrial Ca²⁺ signalling (Pitter et al., 2002; Spät and Pitter, 2004), resulting in enhanced reduction of pyridine nucleotides (Pralong et al., 1992; Rohács et al., 1997) and production of ATP (Tarasov et al., 2012). Moreover, the mitochondrial Ca²⁺ signal and NAD(P)H formation within mitochondria are essential for the hypersecretion of aldosterone (Spät et al., 2012; Wiederkehr et al., 2011).

The soluble adenylyl cyclase (sAC, encoded by *ADCY10*), a cAMP-generating enzyme activated by HCO₃⁻ (Chen et al., 2000; Lefkimmatis et al., 2013; Steegborn et al., 2005b) and Ca²⁺ (Jaiswal and Conti, 2003), is present in the mitochondrial matrix (Acin-Perez et al., 2009b). Mitochondrial Ca²⁺ signals result in enhanced sAC-mediated formation of cAMP within the mitochondrial matrix of HeLa cells and rat cardiomyocytes (Di Benedetto et al., 2013, 2014), as well as in human adrenocortical H295R cells (Katona et al., 2015). In addition to the increased formation of ATP (Acin-Perez et al., 2009b; Di Benedetto et al., 2013; Wang et al., 2016), mitochondrial cAMP (mt-cAMP) may have cell type-specific roles, as exemplified by the reduced aldosterone production in adrenocortical cells after the knockdown of sAC (Katona et al., 2015). Mitochondrial Ca²⁺ is one of the key regulators of aldosterone synthesis (Wiederkehr et al., 2011), and it also boosts pyridine nucleotide reduction, which may also favour steroid production (Pralong et al., 1992; Spät et al., 2012). Therefore, in the present study, we examined whether the hormone secretion-promoting action of mt-cAMP reflects an effect on mitochondrial Ca²⁺ handling itself. We show that mt-cAMP enhances mitochondrial Ca²⁺ uptake and boosts the subsequent hormonal response in H295R human adrenocortical cells. The effect of mt-cAMP on mitochondrial Ca²⁺ handling is not mediated by changes in the mitochondrial membrane potential ($\Delta\Psi_m$) or Ca²⁺ efflux, but requires the cAMP-regulated guanine nucleotide exchange factor Epac1 (also known as RAPGEF3). Importantly, this feedback mechanism was also detected in HeLa cells, showing that it is not confined to steroid-producing cells.


RESULTS

Inhibition of mt-cAMP formation attenuates mitochondrial Ca²⁺ accumulation during Ca²⁺ signalling in intact H295R cells

First, we examined the effects of 2-OHE, a membrane-permeable sAC inhibitor (Steegborn et al., 2005a), on Ca²⁺ signalling in AngII-stimulated H295R cells. The drug significantly reduced the mitochondrial Ca²⁺ uptake rate without a similar effect on the cytosolic response (Fig. S1A). Further experiments, however, revealed that 2-OHE reduces the fluorescence of the membrane potential-sensitive dye TMRM both in the mitochondria and the nuclei (Fig. S1B). 2-OHE failed to influence $\Delta\Psi_m$ in permeabilized cells (Fig. S1C,D), suggesting that the reduction of TMRM

¹Department of Physiology, Semmelweis University Medical School, 1482 POB 2 Budapest, Hungary. ²MTA-SE Laboratory of Molecular Physiology, Semmelweis University and Hungarian Academy of Sciences, 1482 POB 2 Budapest, Hungary.

*Authors for correspondence (spat.andras@med.semmelweis-univ.hu; szanda.gergo@med.semmelweis-univ.hu)

 G.S., 0000-0002-1308-7593; É.W., 0000-0001-8698-6867

fluorescence in intact cells was due to plasma membrane depolarization. Nevertheless, we regarded the results obtained with 2-OHE in AngII-stimulated intact cells as inconclusive.

H295R cells show a voltage-dependent Ca^{2+} influx with an ensuing mitochondrial Ca^{2+} signal when stimulated with K^+ (Szanda et al., 2006). Knocking down sAC with a verified siRNA sequence (MR2; Di Benedetto et al., 2013; Katona et al., 2015 and Fig. S2D) significantly reduced the net mitochondrial Ca^{2+} uptake rate without any effect on cytosolic Ca^{2+} response in K^+ -stimulated cells (Fig. 1A,B). Importantly, knockdown of sAC slightly hyperpolarized mitochondria both under resting conditions and during Ca^{2+} signalling as compared to what was seen in control cells (Fig. 1C). Since hyperpolarization of the mitochondria would increase, rather than decrease, the mitochondrial Ca^{2+} uptake rate, these findings strongly suggest that attenuating mt-cAMP formation impedes mitochondrial Ca^{2+} uptake in a $\Delta\Psi_m$ -independent manner.

Manipulation of the mt-cAMP system in permeabilized cells influences mitochondrial Ca^{2+} accumulation independently of $\Delta\Psi_m$

With the aim of minimizing the effect of extramitochondrial factors, next we analysed the mt-cAMP dependence of mitochondrial Ca^{2+} uptake in permeabilized cells in which perimitochondrial $[\text{Ca}^{2+}]_c$ can be adjusted. 2-OHE was used to inhibit sAC, and erythro-9-(2-hydroxy-3-nonyl)adenine (EHNA), a selective inhibitor of PDE2A (Acin-Perez et al., 2011) and, as such, an enhancer of mt-cAMP formation in H295R (Katona et al., 2015) and HeLa cells (Di Benedetto et al., 2013), was applied to increase [mt-cAMP]. Ca^{2+} accumulation was significantly dampened by 2-OHE (Fig. 2A) and

EHNA markedly accelerated the uptake (Fig. 2B). These observations were corroborated by the finding that the knockdown of sAC reduced mitochondrial Ca^{2+} uptake into the mitochondria of permeabilized H295R cells (Fig. 2C), and we observed a similar reduction of Ca^{2+} uptake in permeabilized sAC-silenced HeLa cells (Fig. 2D).

The sAC- Ca^{2+} interplay was further investigated by combining treatment with a cAMP analogue and sAC silencing. The membrane-permeable cAMP analogue 8-Br-cAMP strongly intensified mitochondrial Ca^{2+} accumulation (Fig. 3A) without any measurable effect on $\Delta\Psi_m$ (Fig. 3B), supporting the notion that mt-cAMP enhances mitochondrial Ca^{2+} accumulation independently of $\Delta\Psi_m$. Moreover, 8-Br-cAMP increased mitochondrial Ca^{2+} uptake to comparable levels in both the control and sAC-silenced permeabilized H295R cells (Fig. 3C), implying that cAMP is a downstream effector of sAC.

Overexpression of sAC in the mitochondrial matrix accelerates mitochondrial Ca^{2+} uptake and intensifies aldosterone secretion

In order to study the effect of increased mt-cAMP formation on Ca^{2+} handling, we generated wild-type (WT) and enzymatically inactive mitochondrially targeted versions of sAC. H295R cells express the truncated (~48 kDa) form of sAC, which localizes predominantly to the particulate fraction (Katona et al., 2015). Although the full-length sAC mRNA (NM_018417.5; 4832 bp CDS) can be found in these cells (Fig. S2A), for our mitochondria-targeted constructs, we used the sequence of the physiologically occurring and enzymatically enhanced truncated version of sAC (Buck et al., 1999; Steegborn, 2014) (Figs S2B, S3 and S4). Interestingly, two

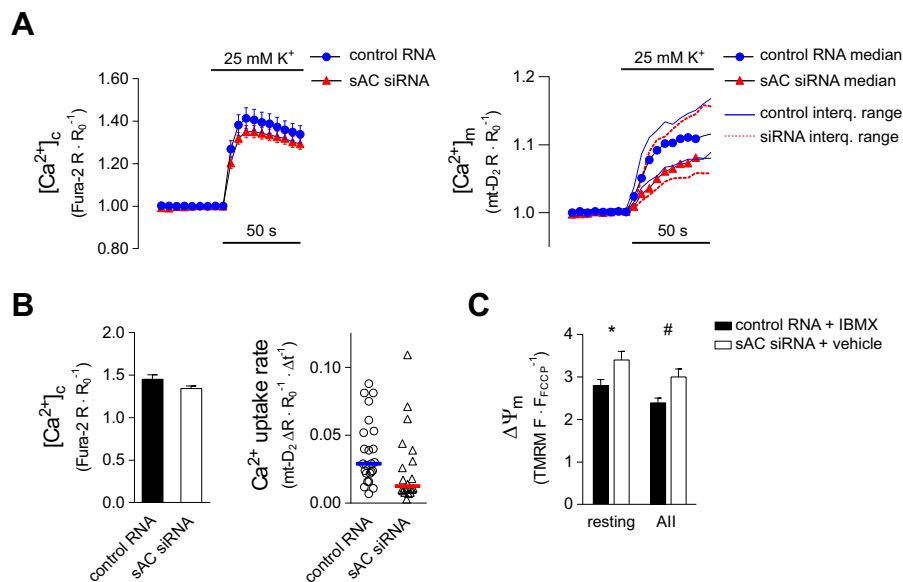


Fig. 1. K^+ -evoked cytosolic and mitochondrial Ca^{2+} signals in sAC-silenced H295R cells. (A) $[\text{Ca}^{2+}]_c$ and $[\text{Ca}^{2+}]_m$ in K^+ -stimulated control (blue circles) and sAC siRNA transfected cells (red triangles). Cells were transfected with the mitochondria-targeted ratiometric probe 4mt-D₂-cpV (mt-D₂) and with siRNA against sAC or control siRNA (non-silencing) and loaded with Fura-2 AM (100 or 500 nM) for 30 min. Fura-2 ($[\text{Ca}^{2+}]_c$) and mt-D₂ ($[\text{Ca}^{2+}]_m$) ratios (R) were normalized to baseline values (R_0). Following a control superfusion period, the cells were stimulated with 25 mM K^+ . The mitochondrial Ca^{2+} uptake rate is non-Gaussian distribution and, accordingly, the mean and median of $[\text{Ca}^{2+}]_m$ considerably deviated from one another (not shown). Therefore, the left panel shows the mean \pm s.e.m. and the right panel shows median values with interquartile range. For statistics see B. (B) Statistical analysis of K^+ -evoked peak cytosolic Ca^{2+} signals (left) and mitochondrial Ca^{2+} uptake rates (right). The graph on the right shows individual data points and median value (horizontal lines); $n=24$ and 20 for control and sAC siRNA-treated cells, respectively. Significance for uptake rate: $P=0.028$ (Kolmogorov–Smirnov test). (C) Mitochondrial membrane potential ($\Delta\Psi_m$) under resting conditions or Ca^{2+} signalling in cells with different mt-cAMP status. Control cells (elevated [mt-cAMP]) were transfected with non-silencing siRNA and were exposed to the PDE inhibitor IBMX (100 μM , 30 min), whereas cells transfected with sAC siRNA (reduced [mt-cAMP]) were exposed to solvent (0.1% DMSO, 30 min). Following a 2 min control period, cells were exposed to AngII (All, 10 nM) for an additional 2 min before $\Delta\Psi_m$ was dissipated with FCCP+oligomycin. TMRM, IBMX or vehicle were present throughout the entire experiment. $n=37$ control RNA and 39 sAC siRNA-treated cells; * $P=0.0248$, # $P=0.0221$ (two-way ANOVA and Sidak's multiple comparison test).

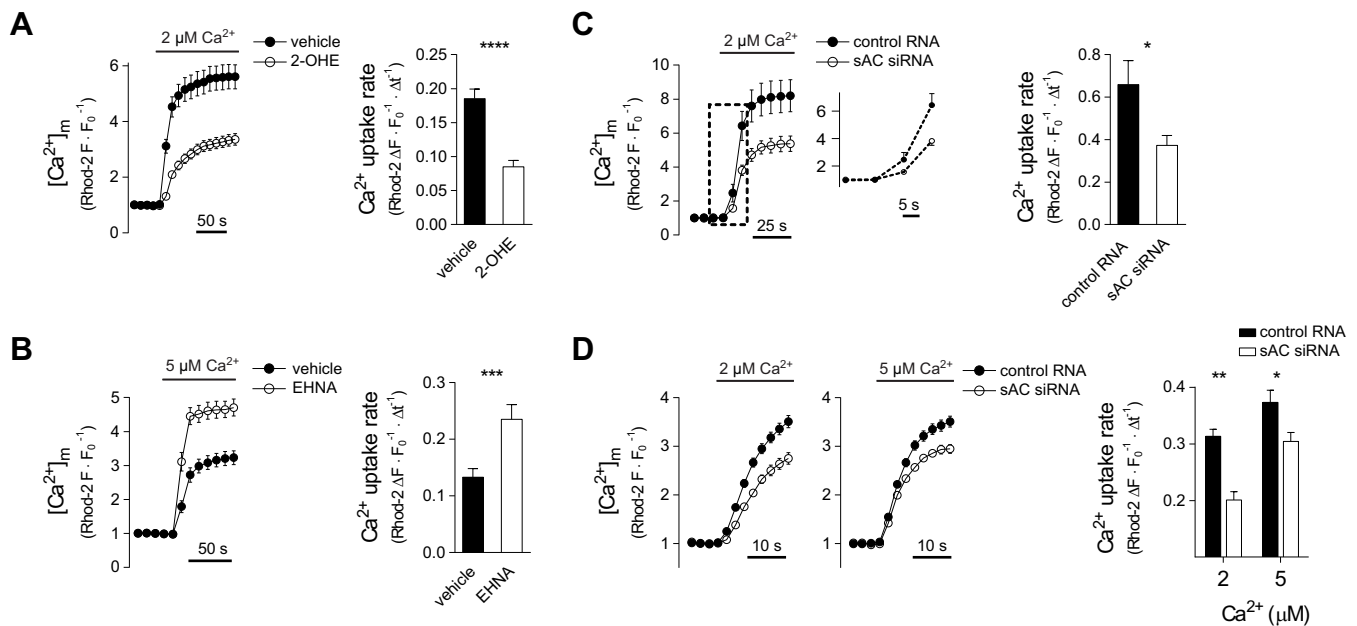


Fig. 2. Effect of mt-cAMP on mitochondrial Ca^{2+} uptake in permeabilized cells. (A,B) Ca^{2+} accumulation into mitochondria of permeabilized H295R cells in the presence of 2-OHE (A) or EHNA (B). Cells were loaded with 2 μM Rhod-2 AM for 30 min at 37°C and then kept at room temperature for 15 min. Following permeabilization, the cells were superfused with Ca^{2+} -free cytosol-like medium and $[\text{Ca}^{2+}]$ was subsequently raised to 2 or 5 μM Ca^{2+} as indicated. Rhod-2 fluorescence data were measured by confocal microscopy and were normalized to that in the control period (F_0). Drugs were present throughout the entire experiment. Column bar graphs show mean mitochondrial Ca^{2+} uptake rates. A: $n=51$ vehicle and 60 2-OHE (20 μM) treated cells; **** $P<0.0001$ (Mann–Whitney test). B: $n=39$ vehicle and 32 EHNA (10 μM) treated cells; *** $P=0.0002$, (Mann–Whitney test). (C) Mitochondrial Ca^{2+} uptake in sAC-silenced permeabilized H295R cells. At 2 days after co-transfection with sAC siRNA or control siRNA, and mitochondrially targeted GFP, dye loading, permeabilization and confocal microscopy were carried out as described for A. After the control period, the $[\text{Ca}^{2+}]$ of the cytosol-like medium was raised from 0 nM to 2 μM as indicated. Only GFP⁺ cells were regarded as RNA-transfected and used for statistics. Column bar graphs show mean mitochondrial Ca^{2+} uptake rate. $n=19$ control and 18 sAC silenced cells; * $P=0.0279$ (*t*-test with Welch’s correction). The section highlighted by the dashed box is magnified on the right. (D) Mitochondrial Ca^{2+} uptake in sAC-silenced permeabilized HeLa cells. At 2 days after transfection with control or sAC siRNA, dye loading, permeabilization and confocal microscopy were carried out as described for C. The $[\text{Ca}^{2+}]$ of the cytosol-like medium was raised from 100 nM to 2 or 5 μM as indicated. Column bar graphs show the mean mitochondrial Ca^{2+} uptake rate. $n=40$ control and 23 sAC-silenced cells at 2 μM $[\text{Ca}^{2+}]$, and 26 control and 40 sAC-silenced cells at 5 μM $[\text{Ca}^{2+}]$; * $P=0.0067$, ** $P<0.0001$ (two-way ANOVA and Sidak’s *post-hoc* test).

sAC isoforms were consistently amplified from H29R cells; one corresponding to the canonical sequence and the other lacking a short section ($\Delta 215\text{--}276$; Fig. S5A) from the C1–C2 region, which links the two catalytic domains (Steegborn, 2014).

In order to obtain functionally compromised mutants, two amino acid changes were introduced (Fig. S2B). In the double mutant sAC the D99A mutation aims to eliminate Mg^{2+} binding, and N412A to abolish ribose binding (Steegborn, 2014). As expected, HeLa cells expressing double mutant mitochondrial sAC (mt-sAC) exhibited significantly reduced mt-cAMP production during Ca^{2+} signalling or when stimulated with HCO_3^- , a direct activator of sAC (Chen et al., 2000; Steegborn, 2014) (Fig. S2C).

If mt-cAMP intensifies mitochondrial Ca^{2+} uptake then one would expect a reduced Ca^{2+} accumulation when an enzymatically inactive sAC is overexpressed in mitochondria. This was indeed the case, as the overexpression of the double mutant mt-sAC markedly reduced the rate of mitochondrial Ca^{2+} accumulation in both permeabilized H295R and HeLa cells as compared to what was seen upon overexpression of the WT cyclase (Fig. 4A,B). [We obtained identical results with the adrenocortical isoforms of sAC (Fig. S5B), strongly suggesting that the linker region is indeed dispensable for the enzymatic activity.] Moreover, the difference in Ca^{2+} uptake rate between WT and mutant sAC was also preserved in the presence of the $\text{Na}^+/\text{Ca}^{2+}$ exchanger (NCLX) blocker CGP-37157 (Fig. S6). In order to test the effect of mt-cAMP-dependent enhancement of Ca^{2+} uptake on the biological response of adrenocortical cells, namely

steroid synthesis, we measured basal and AngII-stimulated aldosterone production in cells transfected with WT or mutant mt-sAC over 2 h (Fig. 4C). Cells expressing mutant mt-sAC showed less steroidogenesis (as compared to WT mt-sAC-expressing counterparts) highlighting the contribution of mt-cAMP to the hormonal response.

The role of Epac1 and protein kinase A in mediating the mt-cAMP effect on Ca^{2+} uptake

Next we studied the involvement of recognized cAMP effectors, protein kinase A (PKA) and the guanine nucleotide exchange (GEF) factor Epac1, in conveying the enhancing effect of mt-cAMP on Ca^{2+} uptake. ESI-09, a pan-Epac inhibitor (Almahariq et al., 2013) reduced mitochondrial Ca^{2+} uptake rate in permeabilized H295R cells (Fig. 5A). In view of data confirming (Zhu et al., 2015) or challenging the specificity of ESI-09 (Rehmann, 2013), we also examined the effect of the structurally unrelated Epac1 inhibitor CE3F4 (Courilleau et al., 2012). This drug also decelerated mitochondrial Ca^{2+} uptake in permeabilized as well as in AngII-stimulated intact H295R cells without affecting the cytosolic Ca^{2+} signal (Fig. 5B,C). Importantly, the conventional PKA inhibitor H-89 failed to affect the Ca^{2+} uptake rate but did cause a decrease in the steady-state $[\text{Ca}^{2+}]_m$ in permeabilized cells (Fig. 5B). And finally, the enhancing effect of mt-sAC overexpression on Ca^{2+} uptake was lost if Epac1 was inhibited with CE3F4 (Fig. 5D) strongly suggesting that Epac is downstream of mt-sAC and mt-cAMP. Taken together, these

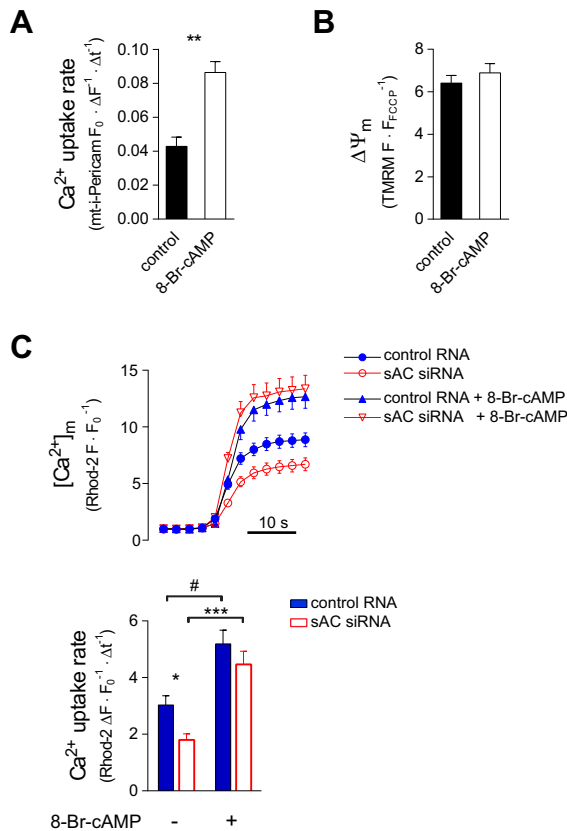


Fig. 3. Mitochondrial Ca^{2+} uptake and $\Delta\Psi_m$ in the presence of 8-Br-cAMP in H295R cells. (A) Effect of 8-Br-cAMP on mitochondrial Ca^{2+} uptake in permeabilized H295R cells. Cells expressing mt-i-Pericam were pre-incubated (37°C) in the presence or absence of 1 mM 8-Br-cAMP for 60 min. Following permeabilization, the cells were incubated with or without 1 mM 8-Br-cAMP for an additional 15 min in a Ca^{2+} -free cytosol-like medium. After the control superfusion period, the $[\text{Ca}^{2+}]_m$ was raised in the medium from 0 to $2\ \mu\text{M}$. Confocal and wide-field fluorescence microscopy measurements of mt-i-Pericam (expressed as F_0/F) gave identical results and therefore data were pooled. $n=36$ control and 56 8-Br-cAMP-treated cells; $**P<0.0001$ (Mann–Whitney test). (B) The effect of 8-Br-cAMP on $\Delta\Psi_m$. Cells were incubated with 8-Br-cAMP, permeabilized and pre-incubated with 8-Br-cAMP again as described for A. $n=123$ control and 85 8-Br-cAMP-treated cells ($P=0.319$, t -test). (C) Effect of 8-Br-cAMP (triangles) on mitochondrial Ca^{2+} uptake in cells transfected with control RNA (solid blue symbols) or sAC siRNA (empty red symbols). Cells were co-transfected with sAC siRNA or control siRNA, and with mitochondrially targeted GFP. Rhod-2 loading, permeabilization and microscopy were performed as described for Fig. 2A and, again, only GFP⁺ cells were regarded as RNA-transfected and used for statistics. After permeabilization, cells were incubated with 1 mM 8-Br-cAMP in Ca^{2+} -free cytosol-like medium for 15 min. Then, cells were superfused with Ca^{2+} -free cytosol-like medium and the perimitochondrial $[\text{Ca}^{2+}]_m$ was raised to $2\ \mu\text{M}$. The upper panel shows mean curves (\pm s.e.m.); the lower panel shows mean mitochondrial Ca^{2+} uptake rate (\pm s.e.m.). The number of observations was: control RNA, 28, control RNA+8-Br-cAMP, 30, sAC siRNA, 18, and sAC siRNA +8-Br-cAMP, 20. $*P=0.0487$, $\#P=0.0143$, $***P=0.0001$ (ANOVA followed by Dunn's post-hoc test).

data strongly suggest that Epac has an essential role in the control of initial Ca^{2+} uptake whereas PKA, acting with a longer lag-time, may contribute to maintaining elevated $[\text{Ca}^{2+}]_m$.

DISCUSSION

Ca^{2+} uptake into mitochondria occurs by diffusion through the voltage-dependent anion channels (VDACs) in the outer mitochondrial membrane followed by the transport through the IMM by the

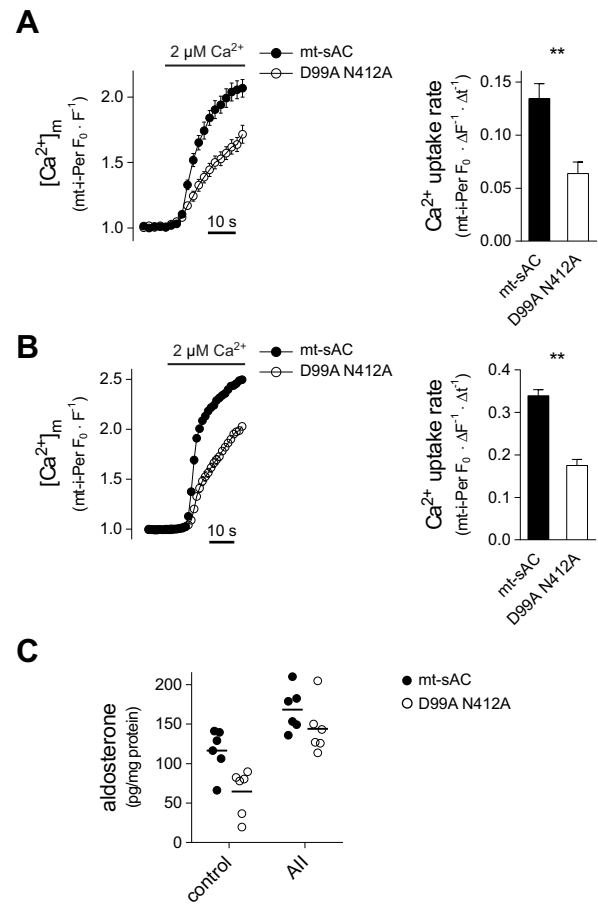


Fig. 4. Effect of mt-sAC overexpression on mitochondrial Ca^{2+} accumulation and aldosterone production. (A) Mitochondrial Ca^{2+} uptake in permeabilized H295R cells expressing WT or mutant mitochondrially targeted sAC. Cells were co-transfected with a plasmid coding the mitochondrially targeted Ca^{2+} sensitive fluorescent protein mt-i-Pericam (mt-i-Per) together with mitochondrially targeted sAC (mt-sAC–mRFP) or the double mutant version (D99A N412A) thereof. At 2 days after transfection, the cells were permeabilized and superfused with a Ca^{2+} -free cytosol-like medium before raising $[\text{Ca}^{2+}]_m$ to $2\ \mu\text{M}$. Pericam fluorescence was measured by confocal microscopy and was normalized to that in the control period and expressed as F_0/F ; only mRFP-positive cells were analysed. Column bar graphs show the mean mitochondrial Ca^{2+} uptake rate. $n=23$ mt-sAC and 19 D99A N412A-expressing cells. $**P<0.0001$ (Mann–Whitney test). (B) Mitochondrial Ca^{2+} uptake in permeabilized HeLa cells expressing WT or mutant mt-sAC variants. Cells were co-transfected with mt-i-Pericam and WT or the double mutant (D99A N412A) mt-sAC–mRFP. For further details see A. The right panel shows average mitochondrial Ca^{2+} uptake rate. $n=76$ WT mt-sAC and $n=57$ double mutant sAC cells. $**P<0.0001$ (Mann–Whitney test). (C) Aldosterone production in H295R cells expressing WT or mutant mt-sAC. Cells were transfected with plasmids coding for WT or double mutant mt-sAC–V5 and basal and AngII (All)-stimulated aldosterone production was measured over 2 h as described in the Materials and Methods. Horizontal lines denote the mean. $P=0.0045$ for WT versus double mutant, $P<0.0001$ for the effect of AngII and $P=0.35$ for the interaction (two-way ANOVA).

mitochondrial Ca^{2+} uniporter (MCU) multiprotein complex, the structure of which has been recently elucidated (MCU, Baughman et al., 2011; De Stefani et al., 2011; MCUB, Raffaello et al., 2013; MICU1, Perocchi et al., 2010; MICU2, Plovanich et al., 2013; EMRE, Sancak et al., 2013; for reviews see, for example, De Stefani et al., 2016; Mammucari et al., 2016). The transport is driven by the 150–180 mV (inside negative) mitochondrial membrane potential (Ψ_m). The ensuing mitochondrial Ca^{2+} signal modulates important

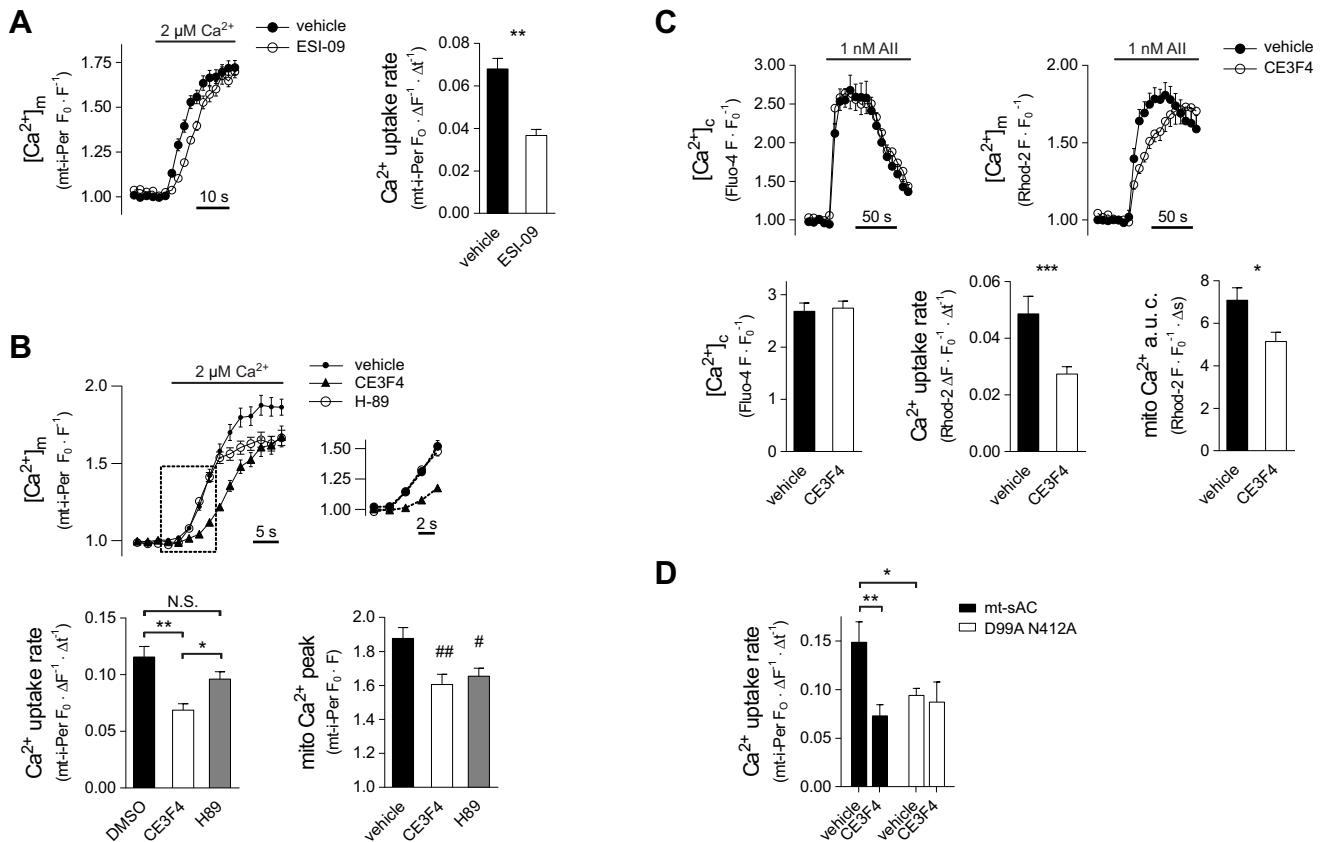


Fig. 5. Role of Epac and PKA in the control of mitochondrial Ca^{2+} uptake. (A) Mitochondrial Ca^{2+} accumulation in permeabilized H295R cells exposed to the pan-Epac inhibitor ESI-09. Cells were pre-incubated with 20 μM ESI-09 or DMSO for 20 min in DMEM/F12 at 37°C. After permeabilization, cells were incubated with 20 μM ESI-09 for a further 10 min in a Ca^{2+} -free cytosol like medium. Following a 30 s Ca^{2+} -free control superfusion $[\text{Ca}^{2+}]$ was raised to 2 μM . mt-i-Pericam (mt-i-Per) fluorescence was measured with a confocal microscope and expressed as F_0/F . Column bar graphs display the mean mitochondrial Ca^{2+} uptake rate. $n=35$ vehicle and $n=28$ ESI-09-treated cells; $**P<0.0001$ (*t*-test). (B) Mitochondrial Ca^{2+} uptake in permeabilized H295R cells in the presence of PKA (H-89) or Epac1 (CE3F4) inhibitors. Cells expressing mt-i-Pericam were pre-incubated with 20 μM CE3F4, 20 μM H-89 or 0.04% DMSO for 1 h in DMEM/F12 at 37°C. After permeabilization, cells were incubated with the appropriate drug for a further 10 min in a Ca^{2+} -free cytosol-like medium. Following a 30 s Ca^{2+} -free control superfusion, $[\text{Ca}^{2+}]$ was raised to 2 μM . Pericam fluorescence was measured with a confocal microscope and expressed as F_0/F . The section highlighted by the dashed box is magnified on the right. The lower left graph displays the mean mitochondrial Ca^{2+} uptake rate whereas the graph on the lower right shows the mitochondrial Ca^{2+} peak. $n=25$, 22 and 23 for vehicle, CE3F4 and H-89-treated cells, respectively. $**P<0.0001$, $*P=0.0439$; $\#P=0.0228$ for vehicle versus H89, and $\#\#P=0.0045$ for vehicle versus CE3F4 (two separate ANOVA analysis both followed by Sidak's post-hoc test). NS, not significant. (C) Effect of Epac1 inhibition on mitochondrial Ca^{2+} handling during AngII (All)-induced Ca^{2+} signalling in H295R cells. For the simultaneous measurement of $[\text{Ca}^{2+}]_{\text{m}}$ and $[\text{Ca}^{2+}]_{\text{c}}$, cells were co-loaded with 2 μM Rhod-2 AM and 2 μM Fluo-4 AM. Then, cells were pre-incubated with 20 μM CE3F4 or vehicle (0.04% DMSO) for 10 min. After a 30 s control superfusion, the cells were exposed to 1 nM AngII. Fluorescence data were monitored by confocal microscopy and normalized to that seen in the 60 s control period. The lower left graph shows the maximal F_0/F Fluo-4 value in the first 60 s of stimulation ($[\text{Ca}^{2+}]_{\text{c}}$ peak); the lower middle graph shows the slope of the linear section of the $[\text{Ca}^{2+}]_{\text{m}}$ curves; the lower right graph shows the area under the curve (a.u.c.) of the $[\text{Ca}^{2+}]_{\text{m}}$ data integrated for the first 60 s of stimulation. $n=19$ vehicle and $n=32$ CE3F4-treated cells. $***P=0.0046$ (unpaired *t*-test), $*P=0.026$ (Mann–Whitney test). (D) Effect of the Epac1 inhibitor CE3F4 on Ca^{2+} uptake in permeabilized HeLa cells. The cells were treated as described for B with the exception that $[\text{Ca}^{2+}]$ was raised from 100 nM (rather than from 0 nM) to 5 μM . $n=19$ and 16, and 27 and 11 for solvent or CE3F4-treated WT sAC transfected cells, and solvent or CE3F4-treated double mutant (D99A N412A) mt-sAC transfected cells, respectively. $**P=0.0037$, $*P=0.0215$, (two-way ANOVA followed by Tukey's *post-hoc* test).

mitochondrial processes as pyridine nucleotide reduction (McCormack et al., 1990), ATP synthesis (Jouaville et al., 1999), apoptosis (Hajnóczky et al., 2000), and even cell type-specific functions including insulin and aldosterone production (Wiederkehr et al., 2011). However, the short-term control of Ca^{2+} uptake under physiologically relevant conditions has remained elusive (De Stefani et al., 2016). In the present study, we reveal a hitherto unrecognized mechanism of this control, specifically that mt-cAMP enhances mitochondrial Ca^{2+} uptake.

Ca^{2+} influx into the mitochondrial matrix activates mt-sAC which, in turn, produces mt-cAMP, a process first described in HeLa cells and cultured cardiac myocytes (Di Benedetto et al., 2013). In our previous study on H295R adrenocortical cells (Katona et al., 2015), we observed that the inhibition or the knockdown of

sAC as well as the buffering of mitochondrial Ca^{2+} by the targeted expression of a Ca^{2+} -binding protein (S100G) significantly reduced AngII-elicited mt-cAMP signalling whereas the inhibition of mitochondrial PDE2A with EHNA (Acin-Perez et al., 2011) enhanced cAMP production within the organelle. The biological significance of mt-cAMP signalling was demonstrated by the reduced aldosterone production after the inhibition or knockdown of sAC. Since $[\text{Ca}^{2+}]_{\text{m}}$ is one of the key factors regulating aldosterone secretion (Spät et al., 2012), in the present study we examined whether the secretagogue effect of mt-cAMP could be mediated by an action of this messenger on mitochondrial Ca^{2+} uptake itself. Moreover, we extended our study of mitochondrial Ca^{2+} handling to HeLa cells so as to assess whether the mt-cAMP– Ca^{2+} interplay is unique to endocrine cells or is a more general phenomenon.

Applying experimental approaches that manipulate mt-cAMP signalling we found that: (1) knockdown of sAC resulted in decelerated mitochondrial Ca^{2+} uptake in intact H295R cells; (2) increasing the mt-cAMP activity through the inhibition of PDE2A, treatment with the cAMP analogue 8-Br-cAMP or by the overexpression of mt-sAC all accelerated Ca^{2+} uptake in permeabilized H295R and HeLa cells; (3) mt-cAMP-dependent changes in mitochondrial Ca^{2+} uptake were not dependent on changes in $\Delta\Psi_m$ or Ca^{2+} efflux; (4) the augmenting effect of mt-cAMP on mitochondrial Ca^{2+} accumulation was sensitive to the inhibition of the Rap GEF Epac1; and (5) overexpressing WT sAC within mitochondria intensified aldosterone production as compared to what was seen for an enzymatically compromised sAC mutant.

Knockdown of sAC decelerated mitochondrial Ca^{2+} accumulation during Ca^{2+} signalling in K^+ -stimulated intact H295R cells. Although sAC in H295R cells locates predominantly to the particulate fraction (Katona et al., 2015), by studying mitochondrial Ca^{2+} uptake in permeabilized cells one may minimize the influence of extramitochondrial factors (Bernardi et al., 1999), and cytosolic cAMP (and quite possibly cytosolic sAC) are also lost under such conditions. Importantly, data obtained in permeabilized cells confirmed the findings in intact cells, as both inhibition and knockdown of sAC impeded Ca^{2+} uptake in H295R and HeLa cells. Moreover, overexpression of WT sAC in the mitochondrial matrix accelerated Ca^{2+} accumulation into the organelle in both cell types.

We found that H295R cells, besides expressing the canonical sAC variant, also express an isoform lacking amino acids 215–276 ($\Delta 215\text{--}276$) within the linker region of the enzyme. This adrenocortical isoform had identical effects on mitochondrial Ca^{2+} uptake as the canonical 48-kDa version, confirming the notion that the linker region is dispensable for enzymatic activity (Steebhorn, 2014). (The deletion in this mutant respects exon–intron boundaries and thus the $\Delta 215\text{--}276$ sAC isoform can probably be regarded as a naturally occurring variant.)

Theoretically, accelerated mitochondrial Ca^{2+} accumulation may reflect increased Ca^{2+} conductance via the MCU, inhibited Ca^{2+} efflux through NCLX, a larger driving force and, naturally, the combination thereof. The maximal rate of mitochondrial Ca^{2+} uptake far exceeds that of Ca^{2+} efflux in H295R cells (A.S. and G.S., unpublished observation) rendering the NCLX an unlikely target of mt-cAMP. Nevertheless, the possibility that mt-cAMP inhibits the NCLX, and thereby accelerates Ca^{2+} accumulation, had to be considered. The enhanced Ca^{2+} uptake in sAC-overexpressing cells was preserved in the presence of CGP-37157, a conventional inhibitor of NCLX. As to the driving force, the membrane-permeable cAMP analogue 8-Br-cAMP increased mitochondrial Ca^{2+} uptake rate but failed to influence $\Delta\Psi_m$. Moreover, knockdown of sAC slightly hyperpolarized mitochondria, yet it reduced the rate of Ca^{2+} accumulation. Taken together, changes in $\Delta\Psi_m$ or Ca^{2+} efflux are not required for the mt-cAMP-dependent modulation of mitochondrial Ca^{2+} handling.

Apart from cyclic nucleotide-activated cation channels in the plasma membrane, two downstream signalling pathways of that are activated by cAMP are generally accepted: activation of PKA and the Epac family of Rap1 exchange factors (Seino and Shibasaki, 2005). The location of PKA within the mitochondrial matrix has not been unambiguously demonstrated. Owing to binding of PKA to several anchoring proteins in the outer mitochondrial membrane and possibly also to the outer surface of the IMM (see Di Benedetto et al., 2013; Lefkimmatis et al., 2013), data on the exact location of PKA in the ‘inner’ mitochondria (Sardanelli et al., 2006; Schwoch

et al., 1990) are not conclusive, and reports on the location of PKA within the matrix are also conflicting (Acin-Perez et al., 2011; Monterisi et al., 2017). There is also no agreement on whether PKA activates the electron transport chain and ATP production (Acin-Perez et al., 2009a; Di Benedetto et al., 2013; Lefkimmatis et al., 2013). In our present study, the conventional PKA inhibitor H89 failed to exert a significant effect on the initial mitochondrial Ca^{2+} uptake. Nevertheless, with some delay, H89 decreased the steady-state $[\text{Ca}^{2+}]_m$. The real biological significance of this latter effect warrants further studies, but the reported off-target effects of H89 should also be kept in mind (Lochner and Moolman, 2006).

Besides PKA, the cAMP-activated GEFs Epac1 and Epac2 (also known as RAPGEF4) are possible mediators of the mt-cAMP effect on mitochondrial Ca^{2+} uptake. The presence of Epac1 in mitochondria (Qiao et al., 2002), in mitoplasts (Wang et al., 2016), in the IMM and also in the matrix (Fazal et al., 2017) has already been documented and an N-terminal mitochondrial target sequence on Epac1 has been identified (Fazal et al., 2017). As to the role of Epac family proteins on mitochondrial Ca^{2+} metabolism, we are aware of two reports on myocardial cells. However, the data are conflicting inasmuch as those of Wang and co-workers (Wang et al., 2016) indicate an inhibitory whereas those of Fazal et al. (Fazal et al., 2017) show a stimulatory effect for the Epac proteins. It should be emphasized that non-physiological conditions were applied in these experiments: mitochondria were isolated from hypertrophic rat hearts (Wang et al., 2016) and mitochondrial Ca^{2+} accumulation in murine cardiac cells was observed in the presence of supraphysiological (50 μM) extramitochondrial Ca^{2+} (without data on the uptake rate) (Fazal et al., 2017). In our experiments a pan-Epac inhibitor and a specific Epac1 inhibitor reduced mitochondrial Ca^{2+} accumulation in intact H295R cells and also in permeabilized H295R and HeLa cells. Moreover, the overexpression of mt-sAC failed to accelerate the mitochondrial Ca^{2+} response in the presence of Epac inhibitors, indicating that Epac1 is the downstream effector of mt-cAMP in this respect. Taken together, whereas the data on cardiac cells (Fazal et al., 2017; Wang et al., 2016) contribute to our knowledge on Epac-dependent cell death, our experiments show that intramitochondrial cAMP and Epac signalling support mitochondrial Ca^{2+} accumulation also at physiological Ca^{2+} concentrations.

Only a small amount of data is available about the role of Epac proteins in the adrenal cortex. A report showing that only ~60% of the cAMP-mediated effects of adrenocorticotrophic hormone (ACTH) on transcription were dependent on PKA in Y1 mouse adrenal cells (Schimmer et al., 2006) gave rise to the idea that the PKA-independent actions were mediated by Epac proteins (Lewis et al., 2016). In murine Y1 cells, the expression of Epac2 could be detected via immunocytochemistry, yet the cell-permeable Epac activator 8-pCPT-2'-O-Me-cAMP failed to simulate the effect of cAMP either on the expression of steroidogenic factors or on steroid secretion over 24 h (Aumo et al., 2010). In bovine glomerulosa cells, both 8-pCPT-2'-O-Me-cAMP and AngII activated the Epac substrate Rap1 but neither of them stimulated aldosterone production over 1 h (Gambaryan et al., 2006). Considering that 8-pCPT-2'-O-Me-cAMP is not resistant to phosphodiesterases (Laxman et al., 2006), its breakdown during cell incubation cannot be ruled out. Owing to well-known species differences in the control of aldosterone secretion (Spät and Hunyady, 2004; Spät et al., 2016), these data should not be extrapolated to human cells. Indeed, our findings showing that knockdown of sAC inhibits (Katona et al., 2015) whereas overexpression of mt-sAC augments aldosterone production, together with the observation that mt-sAC fails to affect mitochondrial Ca^{2+}

uptake in the presence of Epac inhibitors, strongly suggest that mitochondrial Epac is involved in the regulation of the steroidogenic response in the human adrenal cortex.

Conclusion

The combination of work described here and in past studies (Katona et al., 2015) reveals a positive-feedback loop controlling mitochondrial Ca^{2+} handling: Ca^{2+} triggers the formation of mt-cAMP which, in turn, recruits Epac and enhances Ca^{2+} uptake (Fig. 6). This positive feedback is a new example for the convergence of Ca^{2+} and cAMP signalling (Spät et al., 2016). Although excessive function of this system may lead to cell death, it may also have great significance in situations of emergency, especially when a rapid cellular response is required. Changes in basal mt-cAMP metabolism modified the mitochondrial Ca^{2+} uptake rate without a detectable delay, suggesting that even basal mt-sAC activity has a role in triggering the biological response. In case of glomerulosa cells, it can be assumed that during severe salt-water loss (e.g. haemorrhage, diarrhoea and strenuous physical exercise in hot environment) aldosterone secretion is triggered by the simultaneous actions of AngII and corticotrophin (Spät and Hunyady, 2004) and is enhanced by the here-described Ca^{2+} -mt-cAMP- Ca^{2+} positive-feedback system. In addition, given that mt-cAMP also enhances mitochondrial Ca^{2+} uptake in HeLa cells, the present observations may be of broader cell physiological significance.

MATERIALS AND METHODS

Materials

OPTI-MEM, Lipofectamine LTX, RNAiMax, Fluo-4 AM, Rhod-2 AM, tetramethyl rhodamine methylester (TMRM) and Mitotracker Deep Red, as well as the BCA assay kit were purchased from Invitrogen (Thermo Fisher Scientific, Waltham, MA). Fura-2 AM was from Tocris (Ellisville, MO) and

Ultra-MEM was from Lonza (Basel, Switzerland). UltraSer G was from Bio-Septra (Cergy-Saint-Christophe, France). siRNA for silencing sAC (MR2, Di Benedetto et al., 2013) and control siRNA (Universal Negative Control, SIC001) were obtained from Sigma-Aldrich (St Louis, MO). 4mt-H30 was constructed by Giulietta Di Benedetto and Tullio Pozzan (Institute of Neuroscience, Italian National Research Council, Padova, Italy). Mitochondria-targeted inverse Pericam (mt-i-Pericam) was a gift from Atsushi Miyawaki (RIKEN, Saitama, Japan). 4mt-D2 was prepared as described previously (Fülöp et al., 2011). CE3F4 and 8-Br-cAMP was obtained from Cayman (Ann Arbor, MI); other chemicals were obtained from Sigma-Aldrich.

Cell culture and transfection

H295R and HeLa cells were cultured as previously described (Fülöp et al., 2011). Briefly, H295R cells (CRL-2128, ATCC, Manassas, VA) were cultured in Dulbecco's modified Eagle's medium (DMEM)/Ham's F12 (1:1, v/v) supplemented with 1% insulin-transferrin-selenium (ITS⁺), 2% UltraSer G, 100 U ml⁻¹ penicillin and 100 µg ml⁻¹ streptomycin. HeLa cells (CLL-2, ATCC) were grown in DMEM containing 10% heat-inactivated fetal bovine serum (FBS), 100 U ml⁻¹ penicillin and 100 µg ml⁻¹ streptomycin. Passages numbered 3–20 were used. Before experiments, H295R cells were serum-starved overnight (14–16 h) and HeLa cells were starved for 3–5 h. Incubation conditions for aldosterone experiments are described below.

Cells (2.5×10^4 – 5×10^4 H295R or 2×10^4 – 5×10^4 HeLa cells) were plated onto 25-mm diameter circular glass coverslips on day 1 and transfected on day 2 with plasmid DNA (0.5 µg/coverslip except for HeLa cells transfected with 1 µg/coverslip 4mt-H30 DNA) using Lipofectamine LTX (H295R) or Eugene HD (HeLa) according to the manufacturer's protocol. For silencing sAC, on day 2, cells were transfected with 50 pmol MR2 siRNA or control RNA in Ultra-MEM using Lipofectamine RNAiMax. If H295R cells were co-transfected with plasmid DNA and siRNA, RNAiMax was used as the reagent. Experiments were conducted on day 4 or, in case of mt-cAMP measurements, on day 5.

RNA isolation, cDNA preparation and qPCR

RNA isolation and cDNA synthesis were performed as described previously (Ella et al., 2016). For the determination of GAPDH expression by quantitative real-time PCR (qPCR) the LightCycler 480 system (Roche) with the FastStart DNA Master SYBR Green (Roche) was used. Primers were: forward: 5'-AAGGTGAAGGTCGGAGTCAACG-3'; reverse: 5'-GACGGTGCCATGGAATTTGC-3'.

Confocal microscopy

A Zeiss LSM710 confocal laser scanning microscope (operated with ZEN 11.0 software) and a 40*/1.3 water immersion objective (Plan-Apochromat, Zeiss) were used. For monitoring cytosolic and mitochondrial Ca^{2+} signals, the cells were preloaded with Fluo-4 and Rhod-2 or transfected with mt-i-Pericam, as specified in the figure legends. Fluorescence was monitored in multitrack mode; excitation and emission detection wavelengths were set as described previously (Fülöp et al., 2011; Katona et al., 2015). The optical slice was 5 µm in the cytosolic and 3 µm in the mitochondrial channels, but the latter was set at 1.5 µm in the colocalization studies (Figs S2 and S3). In kinetic studies, fluorescence intensity was normalized to the average intensity measured for 20–60 s before stimulation (F_0). The linear section of the normalized Ca^{2+} curves was regarded as rate of Ca^{2+} uptake. Uptake rate was expressed as $(\Delta F/F_0)/\Delta t$ for Rhod-2, or $(F_0/\Delta F)/\Delta t$ in case of mt-i-Pericam.

For the measurement of the mitochondrial membrane potential ($\Delta\Psi_m$), TMRM was used. TMRM (15–25 nM) was present throughout the entire experiment including drug pre-incubation periods. At the end of each run, $\Delta\Psi_m$ was dissipated with 10 µM FCCP+8 µg ml⁻¹ oligomycin and TMRM fluorescence was normalized to that measured after FCCP+oligomycin addition (F_{FCCP}). Excitation and emission were as described previously (Fülöp et al., 2011).

Measurements with fluorescent wide-field microscopy

An inverted microscope (Axio Observer D1, Zeiss) equipped with a 40×1.4 Plan-Apochromat oil immersion objective (Zeiss) and a Cascade II camera (Photometrics) was used for epifluorescence measurements. Mitochondrial

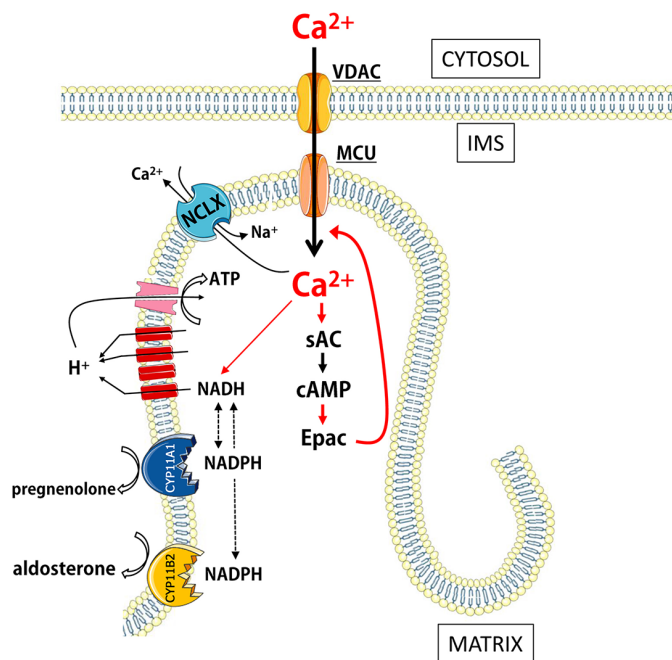


Fig. 6. Schematic illustration of the proposed mt-cAMP-dependent positive feedback control of mitochondrial Ca^{2+} uptake. The main pathway of feedback stimulation: Ca^{2+} entry through the inner mitochondrial membrane into the matrix is followed by increased formation of mt-cAMP that, in turn, enhances Ca^{2+} entry. Red arrows represent activation. See the text for more details. IMS, intermembrane space. Templates from the Servier medical art website (<http://www.servier.com>) were used for this figure.

$[Ca^{2+}]_i$ ($[Ca^{2+}]_m$) and cytosolic $[Ca^{2+}]_c$ ($[Ca^{2+}]_c$) in intact cells were monitored by using 4mt-D₂-cpV (4mt-D₂) and Fura-2, respectively, and $[Ca^{2+}]_m$ in permeabilized cells was monitored with mt-i-Pericam. The mitochondrial Ca^{2+} uptake rate was calculated as described previously (Fülöp et al., 2011). The cAMP level in the mitochondrial matrix was monitored by means of fluorescence resonance energy transfer (FRET), using 4mt-H30 as described previously (Katona et al., 2015).

Superfusion

Microscopic experiments were carried out at room temperature. For kinetic studies in intact cells, the coverslips were superfused with a modified Krebs–Ringer solution containing 140 mM Na⁺, 4.5 mM K⁺, 1.2 mM Ca²⁺, 0.5 mM Mg²⁺, 5 mM HEPES and 2 mM HCO₃⁻ (pH 7.4). Cells were permeabilized with 25 μg ml⁻¹ digitonin in Ca²⁺-free cytosol-like medium (see below) for 6 min. For superfusion of permeabilized cells, a pH 7.1 cytosol-like solution was used containing 129 mM K⁺, 10 mM Na⁺, 1.13 mM Mg²⁺, 120 mM HEPES, 2 mM EGTA, 2 mM ADP, 2 mM pyruvate and 2 mM malate (for H295R) or succinate (for HeLa). To adjust the $[Ca^{2+}]_i$ and $[Mg^{2+}]_i$ of the cytosol-like medium, EGTA, HEDTA, Ca²⁺ and Mg²⁺ were added as calculated by the chelator software (Fabiato, 1988). The flow rate of superfusion was ~1 ml min⁻¹. The solutions were applied with a solenoid valve-equipped gravity-driven superfusion system, terminating at ~2 mm from the selected cells.

Aldosterone measurements

Cells were transfected with the appropriate sAC constructs by means of electroporation (2×10⁶ cells in 100 μl resuspension buffer, 1600 V, 20 ms; Neon Transfection System, Thermo Fisher Scientific) and plated onto 24-well plates (5×10⁵ cells/well) on day 1. Following incubation in the complete medium (see section ‘Cell culture and transfection’), on day 3 the medium was changed to one with 0.1% UltraSer G content for overnight incubation. On day 4, after a 30-min pre-incubation in serum-free medium (supplemented with 0.01% bovine serum albumin), the cells were incubated at 37°C for 2 h in a similar medium, with or without AngII. The aldosterone content of the supernatant and cellular protein amount were determined with a DERCW100 RIA kit (Demeditec, Kiel, Germany) and with a BCA assay (Thermo Fisher Scientific, Waltham, MA), respectively.

DNA constructs

To create the 5mt-sAC-mRFP constructs, the truncated version of soluble adenylyl cyclase (t-sAC, amino acids 1–469) was amplified from serum-deprived human adrenocortical H295R cell cDNA. The following primers were used: forward, 5'-ATATGTCGACGATGAACACTCCAAAAGAA-GAATTCC-3' and reverse, 5'-ATATACCGGTCCTGCTCCGACTTTCT-CAGTACGGCCC-3'. PCR products were digested and cloned into the pmRFP-N1 vector at SalI and AgeI sites. Five consecutive mitochondrial target signals from the human cytochrome *c* oxidase VIII (5 mt) were subcloned at the N-terminal end of sAC. V5- and His-tagged constructs were generated by amplifying the 5mt-sAC section from the above plasmid and cloning into the pcDNA3.1/V5-His TOPO vector (Thermo Fisher Scientific, Waltham, MA). Amino acid changes (D99A, N412A) were introduced by site-directed mutagenesis using the following primers: sAC_D99A forward, 5'-GCAGGTGCTGCACCTGCTAGCC-3'; sAC_D99A, reverse 5'-GCAG-TGCAGCACCTGCAAAATTTCCAGG-3'; sAC_N412A forward, 5'-GTCG-CCTTAGCTGCCAGGATGATGATGACTACTACC-3'; and sAC_N412A reverse, 5'-GGCAGCTAAGGCGACTTTTTGACCAATGACTG-3'. Every construct was verified by sequencing (Microsynth, Balgach, Switzerland).

Statistics

Means±s.e.m. are shown unless otherwise specified. In some experiments, in cases of high-impact outliers, minimal and maximal values have been uniformly excluded in all groups (trimmed mean). In some cases, for better visibility, mean±s.e.m. are shown, and in microscopy experiments with 1 Hz≤acquisition frequency, only every second or third data points are marked by actual symbols. For estimating significance of differences, a Student's unpaired *t*-test, Mann–Whitney and Kolmogorov–Smirnov test, one- and two-way ANOVA and post-hoc tests were used, as appropriate.

Data were analysed with Statistica 13, Microsoft Excel 2016 and GraphPad Prism 5 software.

Acknowledgements

We gratefully acknowledge the valuable discussions with Professors Erzsébet Ligeti, László Tretter and Miklós Geiszt; the excellent technical help of Miss Ágnes Südy and Miss Laura Szalai in the qPCR measurements is highly appreciated.

Competing interests

The authors declare no competing or financial interests.

Author contributions

Conceptualization: G.S., A.S.; Methodology: G.S., É.W.; Formal analysis: A.S.; Investigation: G.S., A.R., A.S.; Resources: G.S.; Writing - original draft: G.S., A.S.; Visualization: G.S.; Supervision: G.S., A.S.; Project administration: G.S., A.S.; Funding acquisition: G.S.

Funding

This work was supported by the following grants: Nemzeti Kutatási és Technológiai Hivatal (National Research, Development and Innovation Office) (grant NKFI-6/FK_124038); Országos Tudományos Kutatási Alapprogramok (Hungarian Scientific Research Fund) (grants 108382 and K116954). The work was also funded by the Magyar Tudományos Akadémia (Hungarian Academy of Sciences). G.S. was supported by the János Bolyai Research Scholarship of the Hungarian Academy of Sciences.

Supplementary information

Supplementary information available online at <http://jcs.biologists.org/lookup/doi/10.1242/jcs.215178.supplemental>

Reference

- Acin-Perez, R., Salazar, E., Brosel, S., Yang, H., Schon, E. A. and Manfredi, G. (2009a). Modulation of mitochondrial protein phosphorylation by soluble adenylyl cyclase ameliorates cytochrome oxidase defects. *EMBO Mol. Med.* **1**, 392–406.
- Acin-Perez, R., Salazar, E., Kamenetsky, M., Buck, J., Levin, L. R. and Manfredi, G. (2009b). Cyclic AMP produced inside mitochondria regulates oxidative phosphorylation. *Cell Metab.* **9**, 265–276.
- Acin-Perez, R., Russwurm, M., Gunnewig, K., Gertz, M., Zoidl, G., Ramos, L., Buck, J., Levin, L. R., Rassow, J., Manfredi, G. et al. (2011). A phosphodiesterase 2A isoform localized to mitochondria regulates respiration. *J. Biol. Chem.* **286**, 30423–30432.
- Almahariq, M., Tsalkova, T., Mei, F. C., Chen, H., Zhou, J., Sastry, S. K., Schwede, F. and Cheng, X. (2013). A novel EPAC-specific inhibitor suppresses pancreatic cancer cell migration and invasion. *Mol. Pharmacol.* **83**, 122–128.
- Aumo, L., Rusten, M., Mellgren, G., Bakke, M. and Lewis, A. E. (2010). Functional roles of protein kinase A (PKA) and exchange protein directly activated by 3',5'-cyclic adenosine 5'-monophosphate (cAMP) 2 (EPAC2) in cAMP-mediated actions in adrenocortical cells. *Endocrinology* **151**, 2151–2161.
- Baughman, J. M., Perocchi, F., Girgis, H. S., Plovanich, M., Belcher-Timme, C. A., Sancak, Y., Bao, X. R., Strittmatter, L., Goldberger, O., Bogorad, R. L. et al. (2011). Integrative genomics identifies MCU as an essential component of the mitochondrial calcium uniporter. *Nature* **476**, 341–345.
- Bernardi, P., Scorrano, L., Colonna, R., Petronilli, V. and Di Lisa, F. (1999). Mitochondria and cell death. Mechanistic aspects and methodological issues [published erratum appears in Eur J Biochem 1999 Oct;265(2):847]. *Eur. J. Biochem.* **264**, 687–701.
- Briet, M. and Schiffrin, E. L. (2010). Aldosterone: effects on the kidney and cardiovascular system. *Nat. Rev. Nephrol.* **6**, 261–273.
- Buck, J., Sinclair, M. L., Schapal, L., Cann, M. J. and Levin, L. R. (1999). Cytosolic adenylyl cyclase defines a unique signaling molecule in mammals. *Proc. Natl. Acad. Sci USA* **96**, 79–84.
- Chen, Y., Cann, M. J., Litvin, T. N., Iourgenko, V., Sinclair, M. L., Levin, L. R. and Buck, J. (2000). Soluble adenylyl cyclase as an evolutionarily conserved bicarbonate sensor. *Science* **289**, 625–628.
- Cherradi, N., Rossier, M. F., Vallotton, M. B., Timberg, R., Friedberg, I., Orly, J., Wang, X. J., Stocco, D. M. and Capponi, A. M. (1997). Submitochondrial distribution of three key steroidogenic proteins (steroidogenic acute regulatory protein and cytochrome p450_{sc} and 3α-hydroxysteroid dehydrogenase isomerase enzymes) upon stimulation by intracellular calcium in adrenal glomerulosa cells. *J. Biol. Chem.* **272**, 7899–7907.
- Courilleau, D., Bisserier, M., Jullian, J.-C., Lucas, A., Bouyssou, P., Fischmeister, R., Blondeau, J.-P. and Lezoualc'h, F. (2012). Identification of a tetrahydroquinoline analog as a pharmacological inhibitor of the cAMP-binding protein Epac. *J. Biol. Chem.* **287**, 44192–44202.
- De Mello, W. C. (2017). Local renin angiotensin aldosterone systems and cardiovascular diseases. *Med. Clin. North Am.* **101**, 117–127.

- De Stefani, D., Raffaello, A., Teardo, E., Szabo, I. and Rizzuto, R. (2011). A forty-kilodalton protein of the inner membrane is the mitochondrial calcium uniporter. *Nature* **476**, 336-340.
- De Stefani, D., Rizzuto, R. and Pozzan, T. (2016). Enjoy the Trip: Calcium in Mitochondria Back and Forth. *Annu. Rev. Biochem.* **85**, 161-192.
- Di Benedetto, G., Scalzotto, E., Mongillo, M. and Pozzan, T. (2013). Mitochondrial Ca²⁺ uptake induces cyclic AMP generation in the matrix and modulates organelle ATP levels. *Cell Metab.* **17**, 965-975.
- Di Benedetto, G., Pardini, D., Greotti, E., Pizzo, P. and Pozzan, T. (2014). Ca²⁺ and cAMP cross-talk in mitochondria. *J. Physiol* **592**, 305-312.
- Ella, K., Csepanyi-Komi, R. and Kaldi, K. (2016). Circadian regulation of human peripheral neutrophils. *Brain Behav. Immun.* **57**, 209-221.
- Fabiato, A. (1988). Computer programs for calculating total from specified free or free from specified total ionic concentrations in aqueous solutions containing multiple metals and ligands. *Methods Enzymol.* **157**, 378-417.
- Fazal, L., Laudette, M., Paula-Gomes, S., Pons, S., Conte, C., Tortosa, F., Sicard, P., Sainte-Marie, Y., Bisserier, M., Lairez, O. et al. (2017). Multifunctional mitochondrial Epac1 controls myocardial cell death. *Circ. Res.* **120**, 645-657.
- Fülöp, L., Szanda, G., Enyedi, B., Várnai, P. and Spät, A. (2011). The effect of OPA1 on mitochondrial Ca²⁺ signaling. *PLoS ONE* **6**, e25199.
- Gambaryan, S., Butt, E., Tas, P., Smolenski, A., Allolio, B. and Walter, U. (2006). Regulation of aldosterone production from zona glomerulosa cells by ANG II and cAMP: evidence for PKA-independent activation of CaMK by cAMP. *Am. J. Physiol. Endocrinol. Metab.* **290**, E423-E433.
- Hajnoczky, G., Csordás, G., Madesh, M. and Pacher, P. (2000). Control of apoptosis by IP(3) and ryanodine receptor driven calcium signals. *Cell Calcium* **28**, 349-363.
- Hattangady, N. G., Olala, L. O., Bollag, W. B. and Rainey, W. E. (2012). Acute and chronic regulation of aldosterone production. *Mol. Cell Endocrinol.* **350**, 151-162.
- Jaiswal, B. S. and Conti, M. (2003). Calcium regulation of the soluble adenylyl cyclase expressed in mammalian spermatozoa. *Proc. Natl. Acad. Sci USA* **100**, 10676-10681.
- Jouaville, L. S., Pinton, P., Bastianutto, C., Rutter, G. A. and Rizzuto, R. (1999). Regulation of mitochondrial ATP synthesis by calcium: Evidence for a long-term metabolic priming. *Proc. Natl. Acad. Sci. USA* **96**, 13807-13812.
- Katona, D., Rajki, A., Di Benedetto, G., Pozzan, T. and Spät, A. (2015). Calcium-dependent mitochondrial cAMP production enhances aldosterone secretion. *Mol. Cell Endocrinol.* **412**, 196-204.
- Laxman, S., Riechers, A., Sadilek, M., Schwede, F. and Beavo, J. A. (2006). Hydrolysis products of cAMP analogs cause transformation of *Trypanosoma brucei* from slender to stumpy-like forms. *Proc. Natl. Acad. Sci. USA* **103**, 19194-19199.
- Lefkimmiatis, K., Lerondi, D. and Hofer, A. M. (2013). The inner and outer compartments of mitochondria are sites of distinct cAMP/PKA signaling dynamics. *J. Cell Biol.* **202**, 453-462.
- Lewis, A. E., Aesoy, R. and Bakke, M. (2016). Role of EPAC in cAMP-mediated actions in adrenocortical cells. *Front. Endocrinol.* **7**, 63.
- Lochner, A. and Moolman, J. A. (2006). The many faces of H89: a review. *Cardiovasc. Drug Rev.* **24**, 261-274.
- Mammucari, C., Raffaello, A., Reane, D. V. and Rizzuto, R. (2016). Molecular structure and pathophysiological roles of the mitochondrial calcium uniporter. *Biochim. Biophys. Acta* **1863**, 2457-2464.
- McCormack, J. G., Halestrap, A. P. and Denton, R. M. (1990). Role of calcium ions in regulation of mammalian intramitochondrial metabolism. *Physiol. Rev.* **70**, 391-425.
- Monterisi, S., Lobo, M. J., Livie, C., Castle, J. C., Weinberger, M., Baillie, G., Surdo, N. C., Musheshe, N., Stangherlin, A., Gottlieb, E. et al. (2017). PDE2A2 regulates mitochondria morphology and apoptotic cell death via local modulation of cAMP/PKA signalling. *Elife* **6**, e21374.
- Perocchi, F., Gohil, V. M., Girgis, H. S., Bao, X. R., McCombs, J. E., Palmer, A. E. and Mootha, V. K. (2010). MICU1 encodes a mitochondrial EF hand protein required for Ca²⁺ uptake. *Nature* **467**, 291-296.
- Pitter, J. G., Maechler, P., Wollheim, C. B. and Spät, A. (2002). Mitochondria respond to Ca²⁺ already in the submicromolar range: correlation with redox state. *Cell Calcium* **31**, 97-104.
- Plovanich, M., Bogorad, R. L., Sancak, Y., Kamer, K. J., Strittmatter, L., Li, A. A., Girgis, H. S., Kuchimanchi, S., De Groot, J., Speciner, L. et al. (2013). MICU2, a paralog of MICU1, resides within the mitochondrial uniporter complex to regulate calcium handling. *PLoS ONE* **8**, e55785.
- Prabhu, S. D. and Frangogiannis, N. G. (2016). The biological basis for cardiac repair after myocardial infarction: from inflammation to fibrosis. *Circ. Res.* **119**, 91-112.
- Pralong, W. F., Hunyady, L., Várnai, P., Wollheim, C. B. and Spät, A. (1992). Pyridine nucleotide redox state parallels production of aldosterone in potassium-stimulated adrenal glomerulosa cells. *Proc. Natl. Acad. Sci. USA* **89**, 132-136.
- Qiao, J., Mei, F. C., Popov, V. L., Vergara, L. A. and Cheng, X. (2002). Cell cycle-dependent subcellular localization of exchange factor directly activated by cAMP. *J. Biol. Chem.* **277**, 26581-26586.
- Raffaello, A., De Stefani, D., Sabbadin, D., Teardo, E., Merli, G., Picard, A., Checchetto, V., Moro, S., Szabo, I. and Rizzuto, R. (2013). The mitochondrial calcium uniporter is a multimer that can include a dominant-negative pore-forming subunit. *EMBO J.* **32**, 2362-2376.
- Rehmann, H. (2013). Epac-inhibitors: facts and artefacts. *Sci. Rep.* **3**, 3032.
- Rohács, T., Nagy, G. and Spät, A. (1997). Cytoplasmic Ca²⁺ signalling and reduction of mitochondrial pyridine nucleotides in adrenal glomerulosa cells in response to K⁺, angiotensin II and vasopressin. *Biochem. J.* **322**, 785-792.
- Rossier, B. C., Bochud, M. and Devuyst, O. (2017). The hypertension pandemic: an evolutionary perspective. *Physiology* **32**, 112-125.
- Sancak, Y., Markhard, A. L., Kitami, T., Kovacs-Bogdan, E., Kamer, K. J., Udeshi, N. D., Carr, S. A., Chaudhuri, D., Clapham, D. E., Li, A. A. et al. (2013). EMRE is an essential component of the mitochondrial calcium uniporter complex. *Science* **342**, 1372-1382.
- Sardanelli, A. M., Signorile, A., Nuzzi, R., Rasmio, D. D., Technikova-Dobrova, Z., Drabota, Z., Occhiello, A., Pica, A. and Papa, S. (2006). Occurrence of A-kinase anchor protein and associated cAMP-dependent protein kinase in the inner compartment of mammalian mitochondria. *FEBS Lett.* **580**, 5690-5696.
- Schimmer, B. P., Cordova, M., Cheng, H., Tsao, A., Goryachev, A. B., Schimmer, A. D. and Morris, Q. (2006). Global profiles of gene expression induced by adrenocorticotropin in Y1 mouse adrenal cells. *Endocrinology* **147**, 2357-2367.
- Schwoch, G., Trinczek, B. and Bode, C. (1990). Localization of catalytic and regulatory subunits of cyclic AMP-dependent protein kinases in mitochondria from various rat tissues. *Biochem. J.* **270**, 181-188.
- Seino, S. and Shibasaki, T. (2005). PKA-dependent and PKA-independent pathways for cAMP-regulated exocytosis. *Physiol. Rev.* **85**, 1303-1342.
- Spät, A. and Hunyady, L. (2004). Control of aldosterone secretion: a model for convergence in cellular signaling pathways. *Physiol. Rev.* **84**, 489-539.
- Spät, A. and Pitter, J. G. (2004). The effect of cytoplasmic Ca²⁺ signal on the redox state of mitochondrial pyridine nucleotides. *Molec. Cell. Endocrin* **215**, 115-118.
- Spät, A., Fülöp, L. and Szanda, G. (2012). The role of mitochondrial Ca²⁺ and NAD(P)H in the control of aldosterone secretion. *Cell Calcium* **52**, 64-72.
- Spät, A., Hunyady, L. and Szanda, G. (2016). Signaling Interactions in the Adrenal Cortex. *Front. Endocrinol.* **7**, 17.
- Steebhorn, C. (2014). Structure, mechanism, and regulation of soluble adenylyl cyclases-similarities and differences to transmembrane adenylyl cyclases. *Biochim. Biophys. Acta* **1842**, 2535-2547.
- Steebhorn, C., Litvin, T. N., Hess, K. C., Capper, A. B., Taussig, R., Buck, J., Levin, L. R. and Wu, H. (2005a). A novel mechanism for adenylyl cyclase inhibition from the crystal structure of its complex with catechol estrogen. *J. Biol. Chem.* **280**, 31754-31759.
- Steebhorn, C., Litvin, T. N., Levin, L. R., Buck, J. and Wu, H. (2005b). Bicarbonate activation of adenylyl cyclase via promotion of catalytic active site closure and metal recruitment. *Nat. Struct. Mol. Biol.* **12**, 32-37.
- Szanda, G., Koncz, P., Várnai, P. and Spät, A. (2006). Mitochondrial Ca²⁺ uptake with and without the formation of high-Ca²⁺ microdomains. *Cell Calcium* **40**, 527-538.
- Tarasov, A. I., Griffiths, E. J. and Rutter, G. A. (2012). Regulation of ATP production by mitochondrial Ca(2+). *Cell Calcium* **52**, 28-35.
- Wang, Z., Liu, D., Varin, A., Nicolas, V., Courilleau, D., Mateo, P., Caubere, C., Rouet, P., Gomez, A.-M., Vandecasteele, G. et al. (2016). A cardiac mitochondrial cAMP signaling pathway regulates calcium accumulation, permeability transition and cell death. *Cell Death Dis.* **7**, e2198.
- Wiederkehr, A., Szanda, G., Akhmedov, D., Matak, C., Heizmann, C. W., Schoonjans, K., Pozzan, T., Spät, A. and Wollheim, C. B. (2011). Mitochondrial matrix calcium is an activating signal for hormone secretion. *Cell Metab.* **13**, 601-611.
- Zhang, X. and Lerman, L. O. (2017). The metabolic syndrome and chronic kidney disease. *Transl. Res.* **183**, 14-25.
- Zhu, Y., Chen, H., Boulton, S., Mei, F., Ye, N., Melacini, G., Zhou, J. and Cheng, X. (2015). Biochemical and pharmacological characterizations of ESI-09 based EPAC inhibitors: defining the ESI-09 "therapeutic window". *Sci. Rep.* **5**, 9344.

Supplementary Information

Fig. S1

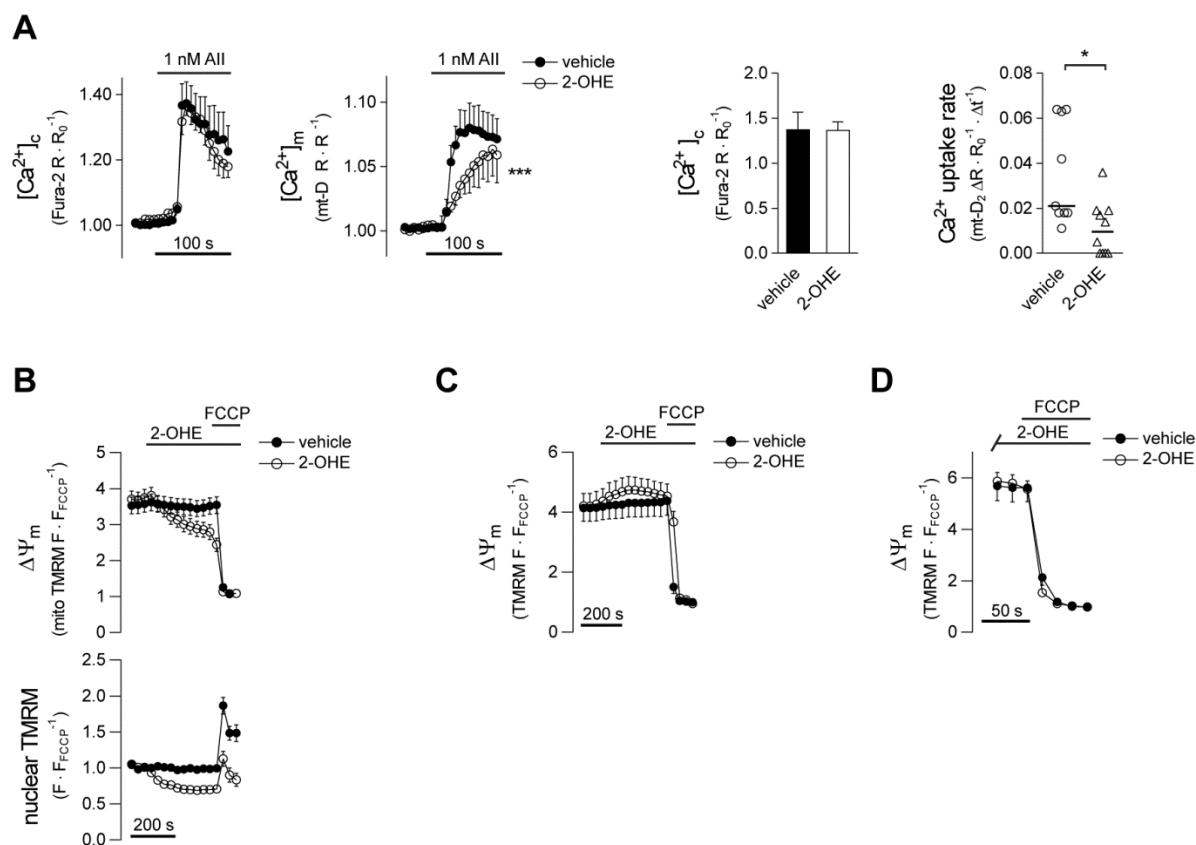


Figure S1. Effect of the sAC inhibitor 2-OHE on mitochondrial Ca^{2+} signalling and $\Delta\Psi_m$ in H295R cells

(A) Simultaneous measurement of $[Ca^{2+}]_c$ and $[Ca^{2+}]_m$ in intact AII-stimulated H295R cells in the presence or absence of the sAC inhibitor 2-OHE (20 μ M). Cells were transfected with the mitochondria-targeted ratio-metric probe 4mt-D₂-cpV (mt-D₂) and loaded with Fura-2 AM (0.1 or 0.5 μ M) for 30 min. Fura-2 ($[Ca^{2+}]_c$) and mt-D₂ ($[Ca^{2+}]_m$) ratios (R) were normalized to baseline values (R₀). Following a control superfusion period, the cells were stimulated with 1 nM AII. Vehicle or 2-OHE was present throughout the entire experiment including dye loading. n = 9 and 10 for vehicle and 2-OHE, resp.; ***p < 0.0001 for the effect of 2-OHE, 2-way ANOVA. The column bar graph shows peak cytosolic Ca^{2+} signal and the dot graph displays initial mitochondrial Ca^{2+} uptake rate. Ca^{2+} uptake rate was determined as the slope of the $[Ca^{2+}]_m$ curve on its linear section. n = 9 and 10 for vehicle and 2-OHE, resp.; *p = 0.012 (Mann-Whitney test). (2-OHE slightly reduced the AII-evoked cytosolic Ca^{2+} response as compared to the vehicle treated group (data not shown). So as to analyse mitochondrial Ca^{2+} signals in the two groups within a comparable range of $[Ca^{2+}]_c$, we excluded control cells (2 out of 11) displaying larger cytosolic Ca^{2+} signals than the maximum seen in the 2-OHE-treated group.) (B) Effect of 2-OHE on mitochondrial (upper graph) and nuclear (lower graph) TMRM fluorescence in intact H295R cells. Cells were loaded with 15 nM TMRM in a modified Krebs-Ringer solution (see *Methods*) at room temperature for 30 min. After loading the cells were exposed to 20 μ M 2-OHE or 0.2% ethanol (vehicle) for 5 min and then to 5 μ M FCCP as indicated. TMRM fluorescence was monitored with confocal microscopy and intensities of mitochondrial regions of interest (ROIs) were normalised to that measured after FCCP addition (F/F_{FCCP}) whereas the nuclear TMRM signal was normalised to the average fluorescence before drug addition (F/F₀). Mean \pm s.e.m. are shown; n = 21 and 20 for vehicle and 2-OHE, resp. (C and D) Effect of 2-OHE on $\Delta\Psi_m$ in permeabilised H295R cells. Cells were permeabilised and then exposed to 2-OHE (20 μ M) or vehicle (0.2% ethanol) for 5 min (C) or 30 min (D) before $\Delta\Psi_m$ was dissipated with 5 μ M FCCP as indicated. TMRM (25 μ M) was present throughout the entire measurement and fluorescence was normalised to that measured after FCCP addition (F/F_{FCCP}). n = 24 2-OHE and 21 vehicle treated cells for *Panel C* and 25 2-OHE and 30 vehicle treated cells for *Panel D*.

Fig. S2

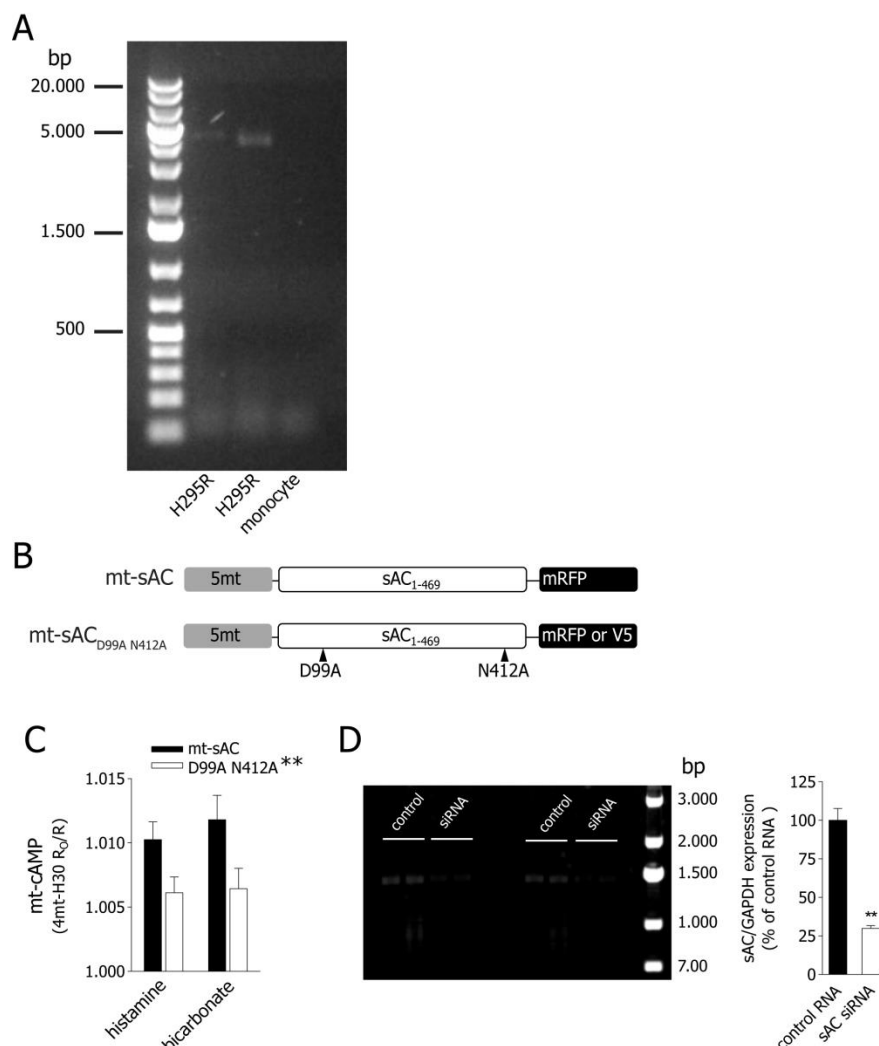


Figure S2. Construction of WT and double mutant sAC isoforms and their effect on mt-cAMP production

(A) PCR revealing the presence of the endogenous canonical full-length sAC mRNA (NM_018417.5; 4832 bp CDS) in H295R cells. Serum starved H295R cells and human peripheral blood monocytes were subjected to RNA isolation and reverse transcription as described in Methods. Primers used:

forward 5' – ATATGTCGACGATGAACACTCCAAAAGAAGAATTCC – 3';

reverse 5' – ATATACCGGTCCTGCTCCGAAATGATTGTCCACGGTATTAGC – 3'.

(B) Schematic domain structure of the mitochondria-targeted truncated sAC constructs. (C) Effect of double mutation on histamine and bicarbonate induced mt-cAMP formation in intact HeLa cells. Cells co-expressing the mitochondrially targeted cAMP sensor 4mt-H30 with WT or double mutant mt-sAC-V5 were kept in a modified Krebs-Ringer medium (see Subsection 2.6) for 30 min at RT. Following a brief control period, the cell were superfused with 5 μ M histamine for 3 min and then with 50 mM HCO₃⁻ for additional 3 min. Fluorescence was monitored by wide-field fluorescent microscopy and 4mt-H30 FRET (CFP/YFP) was normalized to the average measured during control period (R/RO). Bars show the mean maximal R/RO values (+ s.e.m.) detected during histamine and HCO₃⁻ stimulation. n = 28 WT and 21 mutant sAC expressing cells; **p = 0.0041 for the effect of WT vs. double mutant (two-way ANOVA). (D) Knock-down of sAC as verified by PCR. HeLa cells were transfected with sAC-directed siRNA or control dsRNA. Total RNA isolation, reverse transcription and PCR were performed as described in Methods; primers used for amplifying sAC (48 kDa) were as follows:

5' – ATATGTCGACGATGAACACTCCAAAAGAAGAATTCC – 3';

reverse 5' – ATATACCGGTCCTGCTCCGACTTTCTCAGTACGGCCC – 3'.

Expression of sAC was normalized to that of GAPDH. n = 4-4 for both control and siRNA treated; **p = 0.0021, unpaired t-test with Welch's correction.

Fig. S3

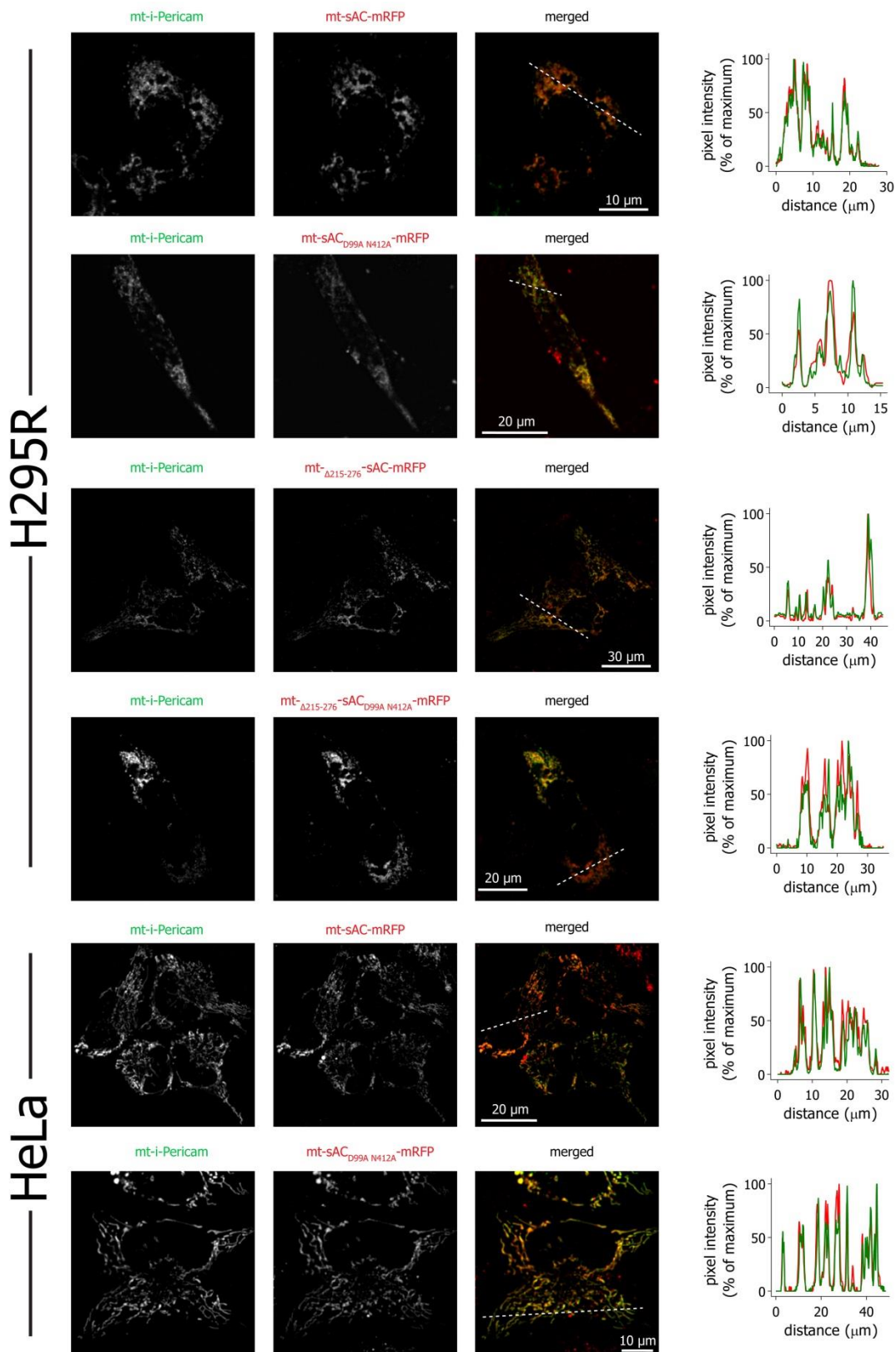


Figure S3. Co-localization of mt-sAC constructs with the mitochondrial Ca^{2+} sensor mt-i-Pericam in intact H295R and HeLa cells

Cells co-transfected with mt-i-Pericam and different mt-sAC constructs were subjected to confocal microscopy as described in *Methods* (but the optical slice was $1.5 \mu\text{m}$). Profiles show fluorescent intensities along a randomly chosen section (dashed line) as normalized to the minimum and maximum (0-100%) values in the pertinent channel. Images are representative for at least 12 cells per mt-sAC construct from at least 2 independent preparations.

Fig. S4

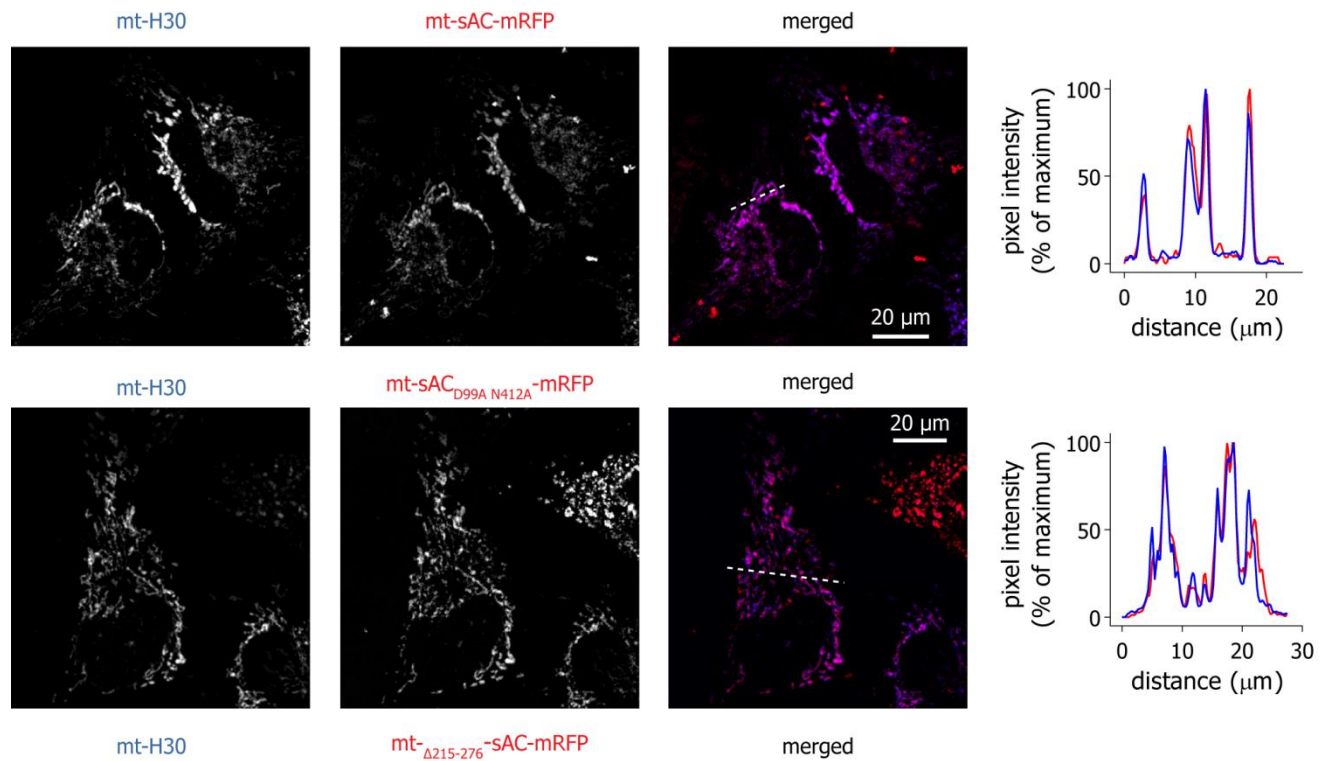
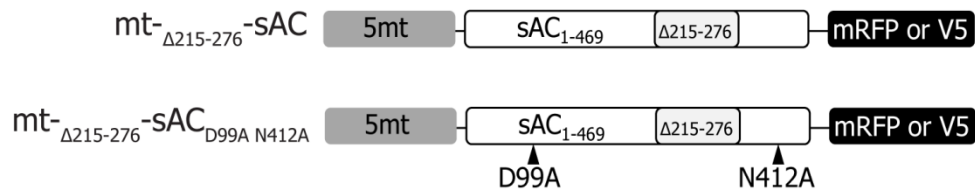


Figure S4. Co-localization of mt-sAC constructs with the mitochondrial cAMP sensor 4mt-H30 in intact HeLa cells

Cells co-transfected with 4mt-H30 and different mt-sAC constructs were subjected to confocal microscopy as described in *Methods* (but the optical slice was 1.5 μm). Profiles show fluorescent intensities along a random line (dashed line) as normalized to the minimum and maximum (0-100%) values in the pertinent channel. Images are representative for at least 9 cells per mt-sAC construct from 2 independent preparations.

Fig. S5

A



B

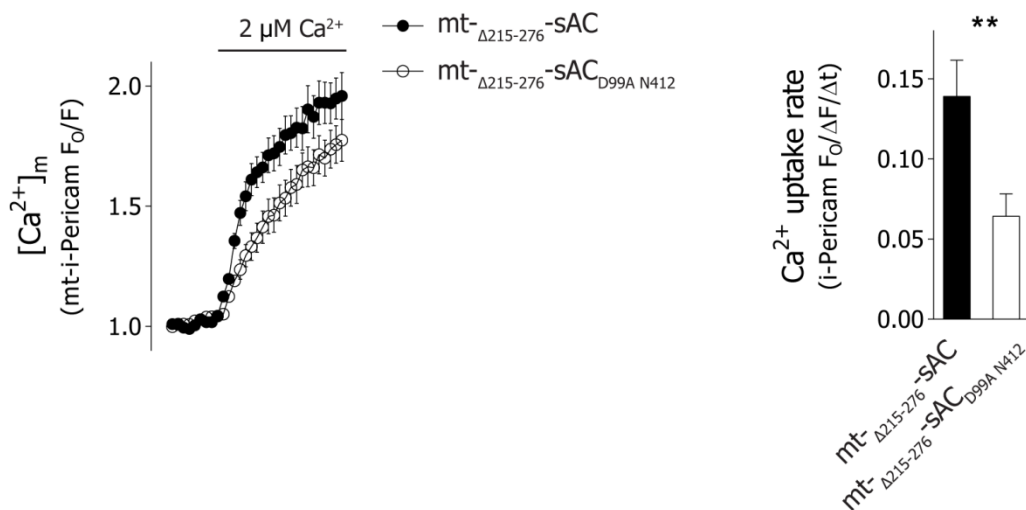


Figure S5. Mitochondrial Ca^{2+} uptake in permeabilised H295R cells expressing the adrenocortical ($\Delta 215-276$) versions of mt-sAC

(A) Schematic domain structure of the mitochondria-targeted adrenocortical-type sAC constructs. (B) Mitochondrial Ca^{2+} uptake was measured in cells co-expressing mt-i-Pericam and WT or double mutant $\Delta 215-276$ mt-sAC-mRFP constructs as described in Fig. 4 A. $n = 15$ WT and 17 mutant expressing cells; $**p = 0.0046$ (Mann-Whitney test).

Fig. S6

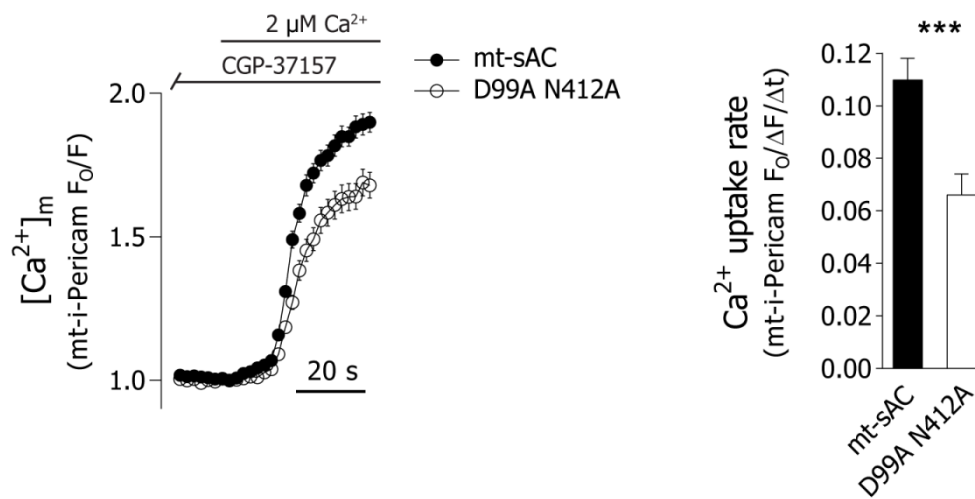


Figure S6. Mitochondrial Ca²⁺ uptake in the presence of the NCLX inhibitor CGP-37157 in HeLa cells

Cells co-expressing mt-i-Pericam and WT or double mutant mt-sAC-mRFP were permeabilised and superfused with Ca²⁺ free cytosol-like medium supplemented with 25 μM CGP-37157 for 220 s before uptake was initiated with 2 μM Ca²⁺. Data collection and analysis was carried out as described in *Fig.4 B*. n = 49 WT and 48 mutant sAC expressing cells; ***p = 0.001 (Mann-Whitney test).